

Spectral analysis of universal conductance fluctuations

I. M. Suslov

P.L.Kapitza Institute for Physical Problems, 119334 Moscow, Russia

E-mail: suslov@kapitza.ras.ru

Universal conductance fluctuations are usually observed in the form of aperiodic oscillations in the magnetoresistance of thin wires as a function of the magnetic field B . If such oscillations are completely random at scales exceeding ξ_B , their Fourier analysis should reveal a white noise spectrum at frequencies below ξ_B^{-1} . Comparison with the results for 1D systems suggests another scenario: according to it, such oscillations are due to the superposition of incommensurate harmonics and their spectrum should contain discrete frequencies. An accurate Fourier analysis of the classical experiment by Washburn and Webb reveals a practically discrete spectrum in agreement with the latter scenario. However, this spectrum is close in shape to the discrete white noise spectrum whose properties are similar to a continuous one. More detailed analysis reveals the existence of the continuous component, whose smallness is explained theoretically. A lot of qualitative results are obtained, which confirm the presented picture. The distribution of phases, frequency differences and the growth exponents agree with theoretical predictions. Discrete frequencies depends weakly on the treatment procedure. The discovered shift oscillations confirm the analogy with 1D systems. Microscopical estimates show agreement of the obtained results with geometrical dimensions of the sample.

1. Introduction

Universal conductance fluctuations [1–4] are usually observed in the form of aperiodic oscillations in the magnetoresistance of thin wires as a function of the magnetic field B [5] (Fig. 1) (see [6, 7] for review). The fluctuation picture looks random, but is completely reproducible from one measurement to another. It is related with a specific realization of the random potential and changes completely, if the sample is heated till sufficiently large temperature, at which the impurities become movable and a new impurity configuration arises (“magnetic fingerprints”).

According to the theory [1–4], the conductance $G(B)$ at a given magnetic field B undergoes fluctuations of the order of e^2/h under the variation of the impurity configuration; fluctuations in $G(B)$ and $G(B + \Delta B)$ are statistically independent, if ΔB exceeds a certain characteristic scale ξ_B . It is reasonable to expect that oscillations in $G(B)$ are completely random at scales exceeding ξ_B . Then, their Fourier analysis should reveal a white noise spectrum (i.e., frequency-independent plateau) at frequencies below ξ_B^{-1} .

Comparison with the results for 1D systems suggests another scenario [8]. A magnetic field perpendicular to a thin wire creates a quadratic potential along this wire [9], which effectively restricts the length of the system L ; hence, the variation of

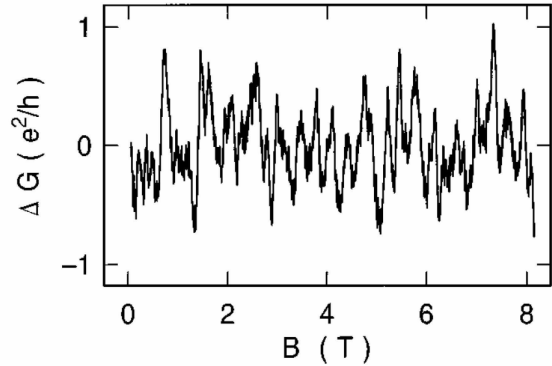


Figure 1: Conductance of the thin Au wire against the magnetic field [5].

the magnetic field is similar to the variation of L . The resistance ρ of a one-dimensional system is a strongly fluctuating quantity and the form of its distribution function $P(\rho)$ essentially depends on the first several moments. Indeed, the Fourier transform of $P(\rho)$ specifies the characteristic function

$$F(t) = \langle e^{ipt} \rangle = \sum_{n=0}^{\infty} \frac{(it)^n}{n!} \langle \rho^n \rangle, \quad (1)$$

which is the generating function of the moments $\langle \rho^n \rangle$. If all moments of the distribution are known, the function $F(t)$ can be constructed using them, and the function $P(\rho)$ is then determined by the in-

verse Fourier transform. If an increase in the moments $\langle \rho^n \rangle$ with n is not too fast, the contributions of higher moments are suppressed by a factor of $1/n!$, whereas first several moments are significant. These moments are oscillating functions of L ,

$$\begin{aligned} \langle \rho \rangle &= a_1(L) + b_1(L) \cos(\omega_1 L + \varphi_1), \\ \langle \rho^2 \rangle &= a_2(L) + b_2(L) \cos(\omega_2 L + \varphi_2) + \\ &+ b_3(L) \cos(\omega_3 L + \varphi_3), \quad \text{etc.}, \end{aligned} \quad (2)$$

where $a_s(L)$ and $b_s(L)$ are monotonic functions. The reason is that the growth exponent for $\langle \rho^n \rangle$ is determined by the $(2n+1)$ th order algebraic equation [8], one of whose root is always real, whereas the other roots are complex for energies in the allowed band. Consequently, there are n pairs of complex conjugate roots. An expression for $\langle \rho^n \rangle$ contains a linear combination of the corresponding exponents, and complex roots provide the existence of n oscillating terms. The frequencies ω_s are usually incommensurate, but their incommensurability vanishes in the deep of the allowed band at weak disorder (Sec. 9). According to this picture, oscillations in $G(B)$ shown in Fig. 1 are determined by the superposition of incommensurate harmonics and their Fourier spectrum should contain discrete frequencies. This picture is indirectly confirmed by the experimental data obtained in [10] and cited in [8], according to which the distribution function $P(\rho)$ is not stationary, but demonstrates systematic aperiodic variations.

It is clear from the above that the Fourier analysis of the function $G(B)$ makes it possible to establish which of two scenarios is more adequate. It will be shown below that such analysis results in the spectrum, which looks purely discrete (Sec. 2), indicating validity of the second conception. Nevertheless, no contradictions arise with the diagrammatic results [1–4], since the form of the spectrum in whole is close to the discrete white noise, whose properties are close to the continuous one. More detailed analysis (Sec. 4) reveals the existence of the continuous component, whose smallness is explained theoretically in Sec. 5. Dependence of results of the treatment procedure is discussed in Sec. 3. In spite of the evident problems, arising due to deviations from the optimal regime, the discrete frequencies of the spectral lines manifest the miraculous stability, proving their objective origin. Analysis of the real and imaginary parts of the Fourier transform $F(\omega)$ of the function $G(B)$ (Fig. 1) reveals the existence of

quick oscillations, related with the shift of B from its "natural" origin, whose nature is discussed in Sec. 6. After exclusion of quick oscillations we study the distribution of phase shifts for the discrete harmonics, which does not contradict their expected stochasticization (Sec. 7). Positions of extrema for $\text{Re}F(\omega)$ and $\text{Im}F(\omega)$ differ from those for $|F(\omega)|$ indicating the existence of the exponential growth of harmonics expected from the analogy with 1D systems (Sec. 8). The distribution of the growth exponents and frequency differences corresponds to the theoretical expectations for the metallic regime (Sec. 9). Microscopical estimates (Sec. 10) indicate an agreement of the presented picture with geometrical dimensions of the sample. A brief communication on the obtained results was published previously [11].

2. Fourier spectrum of aperiodic oscillations

A Fourier analysis of the function $G(B)$ (Fig. 1) cannot be carried out directly, since the abrupt cut-off of experimental data gives rise to slowly decaying oscillations in its spectrum and chaotization of the latter¹. To obtain clear results, it is necessary to use a proper smoothing function. Let us discuss a situation in more details.

Let the function $f(x)$ be the superposition of discrete harmonics and be real. Then,

$$f(x) = \sum_s A_s e^{i\omega_s x} = \frac{1}{2} \sum_s [A_s e^{i\omega_s x} + A_s^* e^{-i\omega_s x}], \quad (3)$$

where the frequencies ω_s can be considered as positive without loss of generality. Then, the Fourier transform of $f(x)$ has the form

$$F(\omega) = \pi \sum_s [A_s \delta(\omega + \omega_s) + A_s^* \delta(\omega - \omega_s)], \quad (4)$$

and its modulus

$$|F(\omega)| = \pi \sum_s |A_s| [\delta(\omega + \omega_s) + \delta(\omega - \omega_s)] \quad (5)$$

depends only on the intensities of spectral lines and

¹ Figure 14 in [5] shows the Fourier spectrum of a thin wire in comparison with the spectrum of a small ring; the latter contains additional oscillations caused by the Aharonov–Bohm effect. However, aperiodic oscillations were not discussed in this place and their spectrum, which is chaotic because of the sharp cutoff, was roughly approximated by the authors in the form of the envelope of oscillations. This is obvious from comparison with Figs. 12 and 13 in [5], where chaotic oscillations are clearly seen.

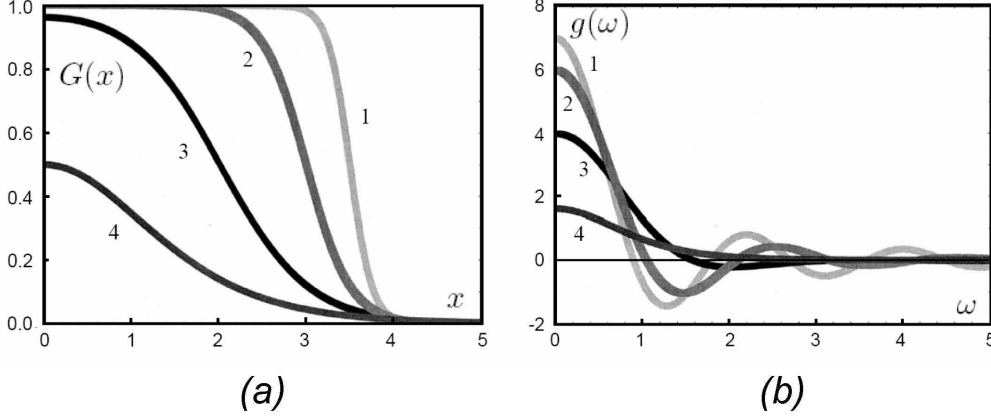


Figure 2: (a) Function $G(x)$ given by Eq. 9, and (b) its Fourier transform $g(\omega)$ at (1) $\mu = 3.5$, $T = 0.125$; (2) $\mu = 3$, $T = 0.25$; (3) $\mu = 2$, $T = 0.5$; and (4) $\mu = T \ln 2$, $T = 0.8$.

does not contain information on phase shifts in the corresponding harmonics. Since $|F(\omega)|$ is an even function, it is possible to consider only positive ω values and to omit the first delta function in Eq. 5.

Since the function $f(x)$ can be experimentally measured only in a finite x range, we in practice have

$$f(x) = \frac{1}{2} \sum_s [A_s e^{i\omega_s x} + A_s^* e^{-i\omega_s x}] G(x), \quad (6)$$

where the function $G(x)$ is unity within the working range and zero beyond it; further, it will be smoothed. Then, instead of Eq. 4, we obtain

$$F(\omega) = \frac{1}{2} \sum_s [A_s g(\omega + \omega_s) + A_s^* g(\omega - \omega_s)], \quad (7)$$

where $g(\omega)$ is the Fourier transform of $G(x)$, which is real for even function $G(x)$. Thus, the restriction of the working range leads to the replacement of delta functions by spectral lines with finite widths. If discrete frequencies are well separated and the function $g(\omega)$ is strongly localized near zero, one can neglect the overlapping of functions $g(\omega \pm \omega_k)$ and write at positive frequencies

$$|F(\omega)|^2 \approx \frac{1}{4} \sum_s |A_s|^2 g^2(\omega - \omega_s). \quad (8)$$

The function $|F(\omega)|^2$ (so-called power spectral density [12]) more adequately characterizes the relative contribution of different harmonics, since the

integral of this function over all frequencies is equal to the integral of $|f(x)|^2$ over all x values. Consequently, change in the spectrum of $f(x)$ at fixed rms fluctuations results in the redistribution of intensities between different frequencies at the conservation of the total spectral power.

It is easy to see that to obtain a clear picture in the case of a discrete spectrum, it is necessary to have a possibly narrower shape of spectral lines determined by $g(\omega)$, which can be achieved by the appropriate choice of the function $G(x)$. The general strategy is determined by the properties of integrals of rapidly oscillating functions [13]. If the function $f(x)$ has discontinuity, its Fourier transform decreases at high frequencies as $1/\omega$; if the n th derivative is discontinuous, then $F(\omega) \sim \omega^{-n-1}$. The Fourier transform of a smooth function $f(x)$ is calculated by shifting the contour of integration to a complex plane and is determined by the nearest singularity or saddle point, which leads to the dependence $F(\omega) \sim \exp(-\alpha\omega)$. If the regular function is obtained by means of a weak smoothing of a singularity, the α value is small and the exponential is manifested only at very high frequencies, whereas the behavior corresponding to the singular function holds in the remaining region. In our case, it is necessary to smooth the discontinuity of $G(x)$. It should be clear that weak smoothing is inefficient, while strong smoothing leads to small values of $G(x)$ near the boundaries of the working range and to loss of experimental information; so, a reasonable compromise is required.

Let $G(x)$ be the x -symmetrized Fermi function

$$G(x) = \frac{1}{1 + e^{(x-\mu)/T} + e^{(-x-\mu)/T}} = \frac{1}{1 + 2e^{-\mu/T} \cosh(x/T)}, \quad (9)$$

whose Fourier transform is given by the integral

$$g(\omega) = \int_{-\infty}^{\infty} \frac{e^{i\omega x} dx}{b \cosh \beta x + c} = \frac{2\pi}{b\beta \sinh x_0} \frac{\sin(\omega x_0/\beta)}{\sinh(\omega\pi/\beta)},$$

$$x_0 = \operatorname{arccosh}(c/b). \quad (10)$$

If $x = B - \mu_0$ is chosen in our case, experimental data correspond to the interval $|x| \leq \mu_0$ with $\mu_0 = 4$ (in units of tesla). As a rule we accepted $\mu = \mu_0 - 4T$, which ensures the small value $G(\mu_0) \approx 0.02$ at boundaries of the interval. As clear from Fig. 2, the behavior $g(\omega) = 2 \sin \mu\omega/\omega$ characteristic of the sharp cutoff prevails at small T values, when smoothing is weak (lines 1 and 2). The extremal smoothing corresponds to $\mu = T \ln 2$, $x_0 = 0$, when

$$g(\omega) = \frac{2\pi T^2 \omega}{\sinh \pi T \omega} \quad (11)$$

and oscillations disappear completely (line 4). It

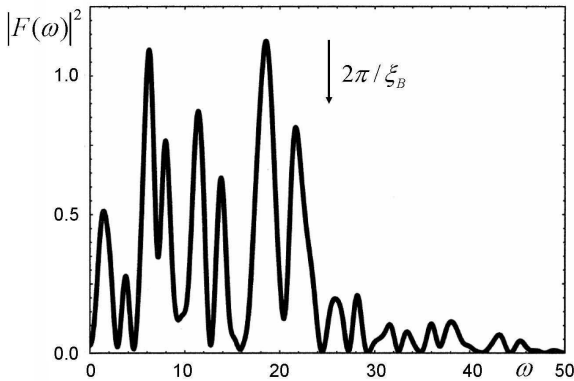


Figure 3: Fourier analysis of the experimental data shown in Fig. 1 for the smoothing function (9) with $\mu = T \ln 2$, $T = 0.8$. Here values of $F(\omega)$ are multiplied by 10, as well as in subsequent figures.

seems reasonable to choose $\mu = 2$ and $T = 0.5$ (line

3), as was made in the paper [11]; in this case, about 50% of experimental data are effectively used, while the line shape is approximately the same as in the case of the extremal smoothing. In the present paper the choice (11) is more convenient; it uses slightly less information but the form of the spectrum is practically the same as in the paper [11].

The spectral analysis of experimental data (Fig. 1) was produced by calculation of the Fourier integral in the region $|x| < \mu_0$ with the indicated smoothing function. The corresponding results are shown in Fig. 3. The spectrum obviously consists of discrete lines, which confirms the second scenario given in beginning. However, the spectrum in the range $\omega \lesssim 2\pi/\xi_B$ (where ξ_B was estimated as the average distance between neighboring maxima or minima in Fig. 1)² is similar to discrete white noise: in a rough approximation, the lines are equidistant and their intensities are more or less the same. Since the sum over frequencies is often approximated by an integral, discrete white noise does not differ in many properties from continuous white noise. Let, for example,

$$F(\omega) = \pi \sum_s [A_s \delta(\omega + \omega_s) + A_s^* \delta(\omega - \omega_s)] H(\omega), \quad (12)$$

where the frequencies ω_s are equidistant ($\omega_s = s\Delta$), the amplitudes A_s are the same in modulus ($|A_s| = A$) and have completely random phases, while $H(\omega)$ is an even function restricting the spectrum to the range $|\omega| \lesssim \Omega$. Then, determining $f(x)$ by means of the inverse Fourier transform, we obtain the correlation function

$$\begin{aligned} \langle f(x)f(x') \rangle &= \frac{1}{2} \sum_s A^2 H^2(\omega_s) e^{i\omega_s(x-x')} \approx \\ &\approx \frac{1}{2} A^2 \Delta^{-1} h(x-x'), \end{aligned} \quad (13)$$

where $h(x)$ is the Fourier transform of $H^2(\omega)$. If the function $H(\omega)$ is smooth, $h(x)$ decreases exponentially at a scale of Ω^{-1} in agreement with the diagrammatic results [1–4].

One can see that the obtained results reconcile two alternative scenarios described at the beginning. On the one hand, the spectrum is practically discrete,

² Under processing, Fig. 1 was strongly magnified and digitized by hand. It was revealed that sharp spikes in Fig. 1 are due to vertical dashes indicating uncertainty of the data, whereas the experimental dependence is in fact smooth.

confirming the picture suggested in [8], where aperiodic conductance oscillations are due to the superposition of incommensurate harmonics. On the other hand, the spectrum as a whole resembles discrete white noise, which is close in properties to continuous white noise.

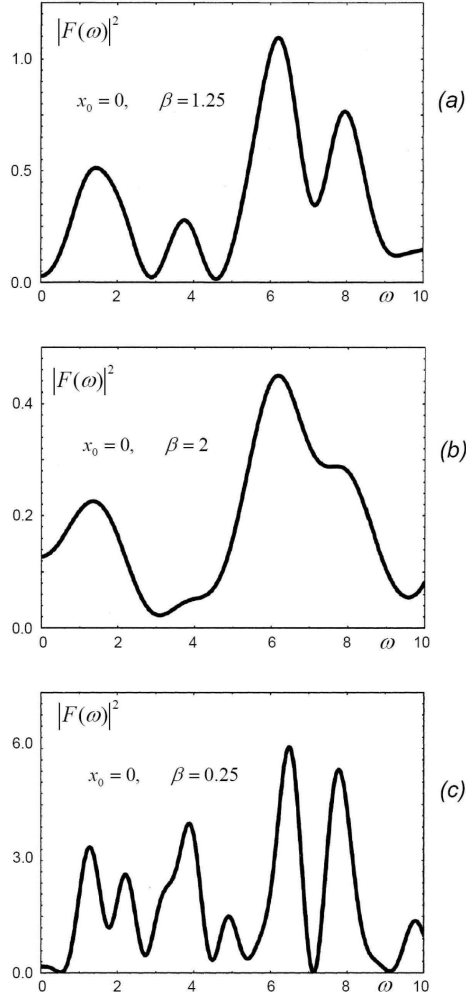


Figure 4: Dependence of the Fourier spectrum on the choice of the smoothing function: (a) $\beta = 1.25$, (b) $\beta = 2.0$, (c) $\beta = 0.25$.

3. Dependence of results on the treatment procedure

Let consider how results are influenced by the choice of the smoothing function (9), which for $\mu = T \ln 2$ leads to the line shape (11) and depends on one

parameter $\beta = 1/T$. For the choice $\beta = 1.25$ it provides the small value $G(\mu_0) \approx 0.02$ at the boundary of the working range and the spectrum of $|F(\omega)|^2$ has a clearly discrete character (Fig. 4,a), which is practically unchangeable in the interval $\beta = 1.0 \div 1.5$. When β is increased, the spectral lines are extended in accordance with (11) and their partial confluence occurs (Fig. 4,b). If β is diminished, then the value $G(\mu_0)$ ceased to be small and the abrupt cutoff is restored, resulting in the appearance of the parasite oscillations and additional maxima of $|F(\omega)|^2$ (Fig. 4,c). The role of the smoothing procedure is exactly in removing such oscillations, which have no relation to the true spectrum.

In spite of the evident problems arising due to deviation from the optimal regime of treatment, the frequencies of the discrete harmonics reveal the surprising stability under the change of β more than the order of magnitude (Fig. 5), and there are no doubts in their objective origin. The small β dependence is related with a change of the shape of spectral lines and their mutual influence by each other. In fact, Fig. 5 demonstrates that approximation of independent harmonics is working sufficiently good.

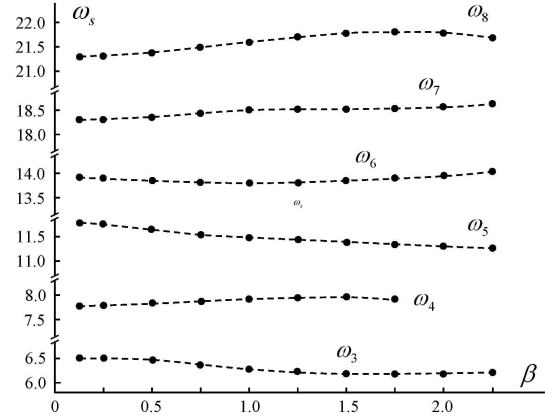


Figure 5: Frequencies of the most intensive harmonics against the parameter $\beta = 1/T$ determining the form of the smoothing function.

If the experimental range of fields was smaller, then the regime of the optimal line resolution (Fig. 4,a) might be absent, and Fig. 4,b with confluent lines would be changed immediately by Fig. 4,c with parasite oscillations. One can suggest, that at the present experimental conditions the line resolution is also incomplete, and they are subjected to

partial confluence.

4. Continuous component of the spectrum

The Fourier spectrum in Fig. 3 looks purely discrete, and it is slightly unnatural. The analogy with 1D systems leads to conclusion that the distribution $P(\rho)$ undergoes systematic variations of deterministic nature leading to the ρ oscillations in the specific sample. However, analogous oscillations (of the random character) should take place even for the stationary distribution $P(\rho)$ due to its finite width. It would be more natural, if Fig. 3 contained the continuous component and the discrete lines were observed against its background. In fact, the continuous component exists actually, and below we try to estimate it.

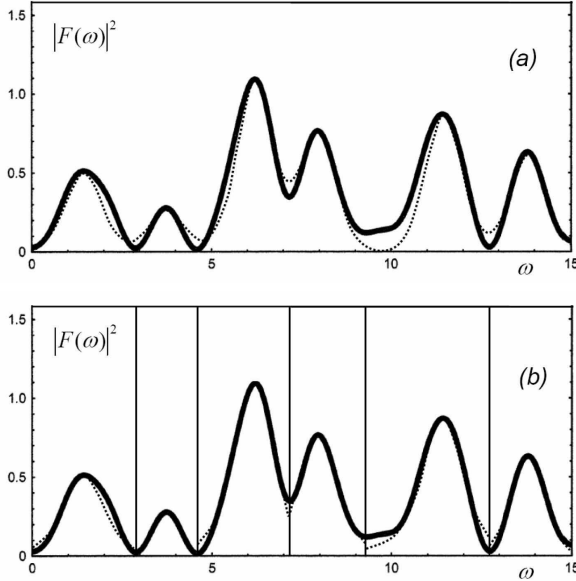


Figure 6: (a) Comparison of the experimental Fourier spectrum (solid line) with relation (8) (dotted line); frequencies ω_s and amplitudes $|A_s|$ were determined by the positions and heights of maxima in Fig. 3. (b) Fitting the form of separate lines according to Eq. 18.

According to (8), in the approximation of independent harmonics the spectrum of $|F(\omega)|^2$ is represented as a superposition of functions $g^2(\omega - \omega_s)$, whose form is known beforehand. The test of relation (8) is presented in Fig. 6,a, where frequencies ω_s and amplitudes $|A_s|$ were determined by the positions and heights of maxima in Fig. 3; no fitting was made in respect of the form of $g^2(\omega - \omega_s)$. Agreement

looks satisfactory, but not complete: the line widths can differ from the theoretical predictions both in the greater or smaller side, while the observed shape of lines is not always symmetric. It is natural to relate these facts with existence of the continuous component of the spectrum. If this component is slowly varied, then counting ω from the line center, one can accept

$$F(\omega) = Ag(\omega) + B, \quad (14)$$

where B is constant on the scale of the line width. Then

$$|F(\omega)|^2 = c_1 g^2(\omega) + c_2 g(\omega) + c_3, \quad (15)$$

where

$$c_1 = |A|^2, \quad c_2 = 2|A||B| \cos \chi, \quad c_3 = |B|^2 \quad (16)$$

and χ is determined by the difference of the A and B phases. If $g(\omega)$ is normalized to unity at $\omega = 0$, then $g^2(\omega)$ corresponds to the more narrow maximum than $g(\omega)$; hence, one has the broadening of the line for $c_2 > 0$ and narrowing for $c_2 < 0$, while the asymmetric form arises if B changes essentially near the maximum. According to (15), $|F(\omega)|^2$ is determined by a superposition of three basis functions $g^2(\omega)$, $g(\omega)$ and 1, whose coefficients may be determined by minimization of rms deviation. This is a standard fitting procedure [12], which is linear and unique. However, practically it leads to nonphysical results due to violation of the condition

$$|c_2| \leq 2\sqrt{|c_1||c_3|}, \quad (17)$$

following from (16). It looks that the optimal fitting corresponds to the limiting values ± 1 for $\cos \chi$; in this case, parameters A and B can be considered as real³, which leads to the equation

$$|F(\omega)|^2 = [(F_0 - B)g(\omega) + B]^2, \quad (18)$$

where $F_0 = |F(0)|$. We have taken into account that the given procedure is reasonable near the maximum of $|F(\omega)|^2$, and its position is naturally kept fixed. Fitting the form of each line according to Eq. 18, we come to Fig. 6,b: agreement is practically ideal for the most of lines, while its absence for some of them

³ It should be stressed that reality of A and B is only effective: in fact, their phases are correlated, being equal to each other or differing by π . It looks that the phases of discrete harmonics are adjusted to a specific realization of the continuous component. The mechanism of this phenomenon is not clear and should be considered as an experimental fact.

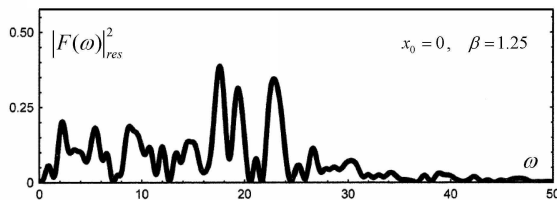


Figure 7: The residual spectrum obtained by exclusion of contributions of the main discrete frequencies. The abrupt maxima are probably related with the secondary harmonics, which were hidden against the background of the main spectral lines. The rest is naturally ascribed to the continuous component.

is probably related with existence of secondary harmonics which were hidden against the background of main lines.

When the coefficients c_1, c_2, c_3 are determined, one can exclude contributions proportional to $g^2(\omega)$ and $g(\omega)$ from $|F(\omega)|^2$. Producing this procedure for all of lines, one comes to the "residual" spectrum presented in Fig. 7. Abrupt maxima in this spectrum are probably related with the secondary discrete harmonics, while the rest part is naturally ascribed to the continuous spectrum; its density corresponds to 10 – 15% of the main lines intensity, and the origin of its smallness is discussed in Sec. 5. The continuous component approximately corresponds to the white noise spectrum for $\omega \lesssim 2\pi/\xi_B$, but the suggested slowness of its variations is not confirmed; hence the obtained result should be considered only as a rough estimate.⁴

Strictly speaking, the quantity B in Eq. 15 represents not only the continuous component, but also the contributions from the neighboring lines. It is not essential for correct estimation of the amplitude A , which is confirmed by analogous calculation for the smoothing function with $\mu = 2, T = 0.5$: the tails of latter are essentially different from those of function (11), while the result is not very different from Fig. 7.

It should be noted, that the spectrum $|F(\omega)|^2$ in Fig. 3 looks "more discrete", than it is such in reality: it is related with the fact that the quantity B , being approximately constant in the vicinity of each maximum, changes its sign in the gaps between

⁴ The treatment procedure is not unique for asymmetric lines, since one can fit their right or left part. This ambiguity was used in order to avoid the appearance of nonphysical negative values for $|F(\omega)|^2_{res}$.

certain lines. The residual spectrum in Fig. 7 does

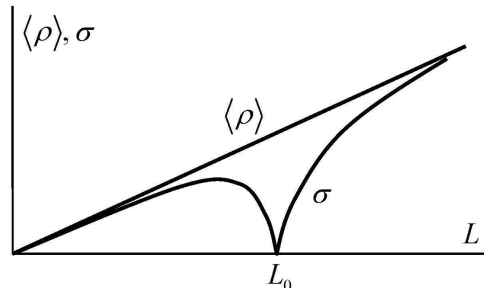


Figure 8: Behavior of $\langle \rho \rangle$ and σ in the metallic regime according to Eq. 19 for the initial condition (22). For the choice $\rho_0 = \langle \rho \rangle$ accepted in the figure, dependence of $\langle \rho \rangle$ against L remains the same as for the initial condition (20). The picture does not change qualitatively, if a typical value from distribution (21) is chosen for ρ_0 .

5. Why the spectrum is practically discrete?

Let us discuss the reasons for smallness of the continuous component of the spectrum. According to [14]-[19], the evolution of distribution $P(\rho)$ in 1D systems is described by the diffusion type equation

$$\frac{\partial P(\rho)}{\partial L} = \alpha \frac{\partial}{\partial \rho} \left[\rho(1+\rho) \frac{\partial P(\rho)}{\partial \rho} \right], \quad (19)$$

where αL plays a role of time. This equation is obtained in the random phase approximation, which is adequate in the quasi-metallic regime, i.e. in the deep of the allowed band for weak disorder [8]. The natural initial condition for (19) has a form

$$P(\rho) = \delta(\rho) \quad \text{for} \quad L = 0, \quad (20)$$

since for the zero length of the system its resistance is zero independently of the random potential realization. Such initial condition leads to the distribution

$$P(\rho) = (\alpha L)^{-1} \exp \{ -\rho/\alpha L \} \quad (21)$$

for small L (when typical values of ρ are small) and to the log-normal distribution at large L (when typical values of ρ are large). The mean value $\langle \rho \rangle$ for distribution (21) coincide with rms deviation σ , while σ grows faster than $\langle \rho \rangle$ in the log-normal regime. Let consider the more general initial condition

$$P(\rho) = \delta(\rho - \rho_0) \quad \text{for} \quad L = L_0, \quad (22)$$

whose meaning is discussed below. Solution of Eq. 19 with the initial condition (22) is close to the Gaussian distribution for L close to L_0 (see Appendix 1), while distribution (21) or the log-normal distribution is restored for large L where the finiteness of ρ_0 and L_0 becomes inessential. When distribution $P(\rho)$ is close to the Gaussian one, it is reasonably described by two first moments, whose evolution is easily obtained (see Appendix 1): the typical situation is presented in Fig. 8. It is easy to see that $\langle \rho \rangle$ is essentially greater than σ in the interval around L_0 , whose width is of order L_0 .

Let discuss the meaning of the initial condition (22). Suppose we are measuring the resistance ρ of the system on the length L_0 , creating different impurity configurations⁵; with sufficiently large number of configurations we shall reproduce distribution (21). Let now change the procedure and select only configurations, whose resistance ρ falls in the small interval around ρ_0 : it artificially creates the ensemble with the narrow distribution of type (22), whose evolution leads to the picture presented in Fig. 8. Let now take a single sample with resistance ρ_0 at the length L_0 . Dependence $\rho(L)$ for this sample can be described theoretically, if all details of the impurity configuration are known. Usually such information is absent, and only general statistical properties of the random potential are available. In this case one can establish only an approximate corridor for possible dependencies $\rho(L)$: this corridor is illustrated by Fig. 8.

Equation (19) is obtained in the random phase approximation, which eliminates all oscillation effects. Fortunately, evolution of $\langle \rho \rangle$ may be investigated exactly without any assumptions (see Appendix 2). In the quasi-metallic regime and for the "natural" ideal leads [8] the following result is valid

$$\langle \rho \rangle = \rho_0 + \frac{1+2\rho_0}{2} \left(e^{2\epsilon^2 l} - 1 \right) + \quad (23)$$

$$+ \frac{\epsilon^2}{\delta} \sqrt{\rho_0(1+\rho_0)} \left[e^{2\epsilon^2 l} \sin \psi - e^{-\epsilon^2 l} \sin(2\delta l + \psi) \right],$$

which was obtained for the discrete Anderson model; here $\delta = k_F a_0$, $\epsilon^2 = W^2/4\delta^2$, $l = (L - L_0)/a_0$, k_F is the Fermi momentum, a_0 is the lattice constant, W is the amplitude of the random potential, and ψ is determined by the difference of phases entering the transfer matrix specified at the scale L_0 . One can

see the existence of oscillations, whose period is determined by the de Brougli wavelegth ($2\delta l = 2k_F L$ for $L_0 = 0$); their amplitude can be comparable with $\rho_0 \ll 1$ in spite of the small parameter ϵ^2/δ . The quantity ψ is completely stochastized in the random phase approximation, and averaging over it eliminates oscillations and restores the result following from Eq. 19 (see (A.6) in Appendix 1). Beyond the metallic regime ($\epsilon^2 \gtrsim \delta$) the amplitude of oscillations is certainly exceeding ρ_0 ,

$$\langle \rho \rangle = \rho_0 + \frac{1}{3} \left(\frac{\epsilon^2}{\delta} \right)^{2/3} \left(\frac{1+2\rho_0}{2} - \cos \psi \sqrt{\rho_0(1+\rho_0)} \right) \cdot$$

$$\cdot \left[e^{x_1 l} - 2 e^{-x_1 l/2} \cos \left(\frac{\sqrt{3} x_1 l}{2} + \frac{\pi}{3} \right) \right], \quad (24)$$

and they do not disappear after averaging over ψ due to fundamental inapplicability of the random phase approximation [8] (here $x_1 = (8\epsilon^2 \delta^2)^{1/3}$). The amplitude of oscillations in the metallic regime increases essentially, when the foreign ideal leads are used,

$$\langle \rho \rangle = \rho_0 + \frac{1+2\rho_0}{2} \left[-1 + \Delta_2^2 e^{2\epsilon^2 l} - \Delta_1^2 e^{-\epsilon^2 l} \cos 2\delta l \right] +$$

$$+ \Delta_1 \sqrt{\rho_0(1+\rho_0)} \cdot \left\{ e^{2\epsilon^2 l} \Delta_2 \cos \psi - \right. \quad (25)$$

$$\left. - e^{-\epsilon^2 l} [(\Delta_2 - 1) \cos \psi \cos 2\delta l + \cos(2\delta l + \psi)] \right\},$$

where Δ_1 and Δ_2 are defined in Appendix 2 and can be large. Thereby, under rather general conditions the amplitude of the $\langle \rho \rangle$ oscillations is comparable with ρ_0 and in the vicinity of L_0 is certainly greater than σ . Unfortunately, results of type (23–25) for higher moments are practically inadmissible due to tremendous calculations, and only general arguments can be given. It is natural to expect, that the second moment $\langle \rho^2 \rangle$ is oscillating with the amplitude of the order of ρ_0^2 , which exceeds essentially the quantity σ^2 . Hence, oscillations of the distribution width due to systematic variations exceed essentially the width of the distribution in the absence of oscillations. As a result, oscillations of higher moments are also essential.

Applicability of the above analysis to the situation under consideration is determined by the fact that the range of fields $B = 2 \div 6T$ was effectively treated for the smoothing function with $\mu = 2$, $\beta = 2$ used in [11], which corresponds to variation of field by a

⁵ It can be made practically by heating the sample till sufficiently high temperature.

factor of three. Since $L \propto B^{-1/2}$, the corresponding variations of L occur⁶ within a factor 1.7. If L_0 is chosen in the middle of the interval, then deviations from L_0 are on the level of 30%. These deviations are even smaller for the smoothing function with $x_0 = 0$, corresponding to (11). The situation does not change, if the experimental range of fields is increasing, because the choice of the smoothing function is determined by the same considerations: only μ_0 value becomes different, while all proportions in Fig. 2 remain unchanged.

6. Shift oscillations

Returning to formulas of Sec. 2, one can see that Eq. 7 is more general than Eq. 8: the former is an exact consequence of Eq. 6, while the latter suggests weak intersection of spectral lines. One can hope that a treatment on the base of Eq. 7 with the use of representation (14) and a separate fitting of the real and imaginary part of $F(\omega)$ provides the more smooth form for $|F(\omega)|_{res}^2$. Unfortunately, these hopes are not confirmed: the obtained picture is not very different from Fig. 7 and does not prove the more complicated treatment. However, study of the real and imaginary parts of $F(\omega)$ reveals a lot of interesting aspects, which are discussed in the present and subsequent sections.

Functions $\text{Re}F(\omega)$ and $\text{Im}F(\omega)$ appear to be quickly oscillating (see Fig. 9,a). The reason of the oscillations is easy to understand: if $F(\omega)$ is the Fourier transform of $f(x)$, then a shift of the x origin leads to the correspondence

$$f(x - a) \iff e^{i\omega a} F(\omega) \quad (26)$$

and the quick oscillations arise for large a . One can puzzle himself by a question on the "natural" choice of the x origin, which corresponds to slow variations of the Fourier transform. Estimating the average period of oscillations in Fig. 9,a, one obtains $a = 4.3$ and elimination of the factor $\exp(i\omega a)$ leads to Fig. 9,b, where $\text{Re}F(\omega)$ and $\text{Im}F(\omega)$ change on the same scale as $|F(\omega)|$. The obtained value of a signifies that the conductance dependence against the magnetic field has a natural origin $B_0 = 8.3T$, which

⁶ The length L is estimated as a value of the x coordinate, for which the quadratic potential $m\omega_B^2 x^2$ [9] becomes of the order of the Fermi energy ϵ_F , so $L \propto B^{-1}$. However, if ϵ_F is comparable with the first Landau level, then it should be replaced by $\hbar\omega_B = \hbar eB/mc$, which gives $L \propto B^{-1/2}$. As clear from Sec. 10, the latter estimate is more adequate near the middle of the experimental range of magnetic fields.

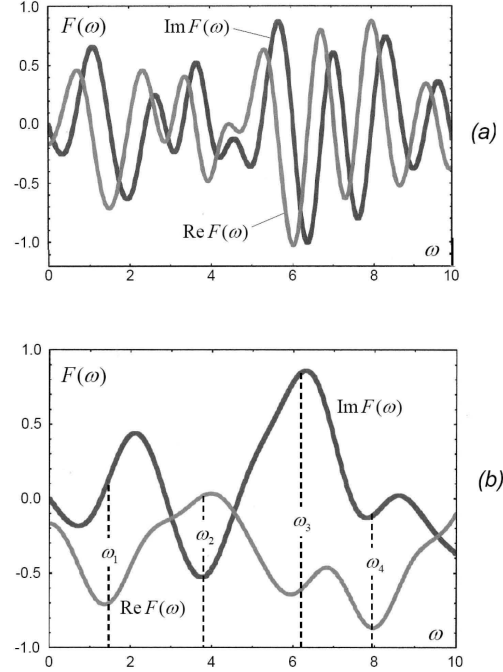


Figure 9: (a) Behavior of the real and imaginary parts of $F(\omega)$ indicates the existence of the shift oscillations $e^{i\omega a}$ with $a = 4.3$; (b) Behavior of $\text{Re}F(\omega)$ and $\text{Im}F(\omega)$ after exclusion of the shift oscillations. Dashed lines indicate the positions of the $|F(\omega)|^2$ maxima.

lies beyond the upper boundary of the experimental range. Since large fields correspond to small system lengths, one can suggest the following interpretation.

When we study the evolution of the distribution $P(\rho)$ against the length L of a 1D system, the natural origin is evidently $L = 0$. However, if evolution begins with a finite scale L_0 , then a form of the distribution at large L appears to be the same as in the case $L_0 = 0$. If we consider a situation at large L and try to extrapolate to the initial stages of evolution, then we cannot establish from which scale it is initiated⁷: we can only claim that this scale is small in comparison with those under consideration. In terms of the magnetic field it means that evolution begins with a certain large value B_0 . However, due to nonlinearity of the relation between L and B the extrapolated B_0 value appears to be not very large⁸.

⁷ Such extrapolation is complicated by the factors, shifting the L origin (see Sec. 5 in [8]).

⁸ As clear from Sec. 5, the main contribution to $F(\omega)$ occurs from the middle of the experimental range of fields, where the relation between L and B is practically linear. Correspond-

Suggested interpretation looks rather logical and provides indirect confirmation of the analogy with 1D systems. The formal arguments on the choice of the natural origin are presented in Appendix 3.

7. The phase distribution

When the natural origin of the argument of $f(x)$ is established, the information on the real and imaginary parts of $F(\omega)$ may be used for a subsequent analysis. Estimating values of $\text{Re}F(\omega)$ and $\text{Im}F(\omega)$

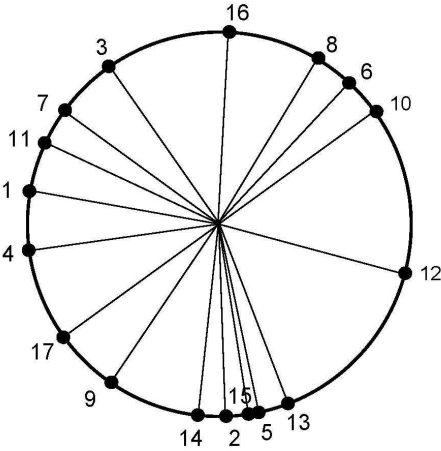


Figure 10: Distribution of the phase factors $e^{i\varphi_s}$ on the unit circle; numbers near points indicate the corresponding s value.

As was discussed in Sec. 2, the discrete white noise is analogous to the continuous one, if phases of A_s are completely random. According to Fig. 10, their distribution is sufficiently uniform and does not contradict to their expected randomness. It would be interesting to verify, how the phase distribution changes when the new impurity configurations are created.

8. Evidence of the exponential growth

According to Eq. 7 contributions of the discrete harmonics to $F(\omega)$ are proportional to $g(\omega - \omega_s)$, and should lead to extrema of the real and imaginary parts of $F(\omega)$ at the points ω_s . However, Fig. 9,b
ingly, extrapolation to the origin is also effectively linear.

demonstrates that extrema of $\text{Re}F(\omega)$ and $\text{Im}F(\omega)$ are realized at different points, not coinciding with maxima of $|F(\omega)|^2$. It indicates invalidity of Eq. 7 and casts doubt on the initial expression (6), from which it was derived.

Let recall that according to Eq. 2 amplitudes of oscillations are not fixed, but subjected to the exponential growth. If the latter is taken into account, then Eq. 6 is modified as

$$f(x) = \frac{1}{2} \sum_s [A_s e^{i\omega_s x + \alpha_s x} + A_s^* e^{-i\omega_s x + \alpha_s x}] G(x), \quad (27)$$

and instead of (7) one comes to the result

$$F(\omega) = \frac{1}{2} \sum_s [A_s g(\omega + \omega_s - i\alpha_s) + A_s^* g(\omega - \omega_s - i\alpha_s)]. \quad (28)$$

Let concentrate on the contribution of the single harmonics ω_s and accept, shifting the ω origin

$$A = A' + iA'' = |A|e^{i\varphi}, \quad g(\omega - i\alpha) = g_1(\omega) + ig_2(\omega). \quad (29)$$

If ω_1 and ω_2 are positions of extrema for $\text{Re}F(\omega)$ and $\text{Im}F(\omega)$, then the following relations are valid

$$\begin{aligned} A'g_1'(\omega_1) - A''g_2'(\omega_1) &= 0, \\ A'g_2'(\omega_2) + A''g_1'(\omega_2) &= 0, \end{aligned} \quad (30)$$

and the phase φ of the coefficient A is determined by the condition

$$\tan \varphi = \frac{g_1'(\omega_1)}{g_2'(\omega_1)} = -\frac{g_2'(\omega_2)}{g_1'(\omega_2)}. \quad (31)$$

If the experimental values of ω_1 and ω_2 are known, then φ and α are determined by the following algorithm. According to Eq. 29, $g_1(\omega)$ and $g_2(\omega)$ depends on α , and $g_2(\omega) \rightarrow 0$ for $\alpha \rightarrow 0$; hence for small α the former fraction in (31) is large, while the latter is small in modulus. Increasing α , one can reach equality in Eq. 31, which determines $\tan \varphi$ and α . The known value of tangent specifies φ to additive contributions multiple of π , and to establish the correct quadrant for φ one can use the relations

$$\begin{aligned} A'g_1(\omega_1) - A''g_2(\omega_1) &= F_1, \\ A'g_2(\omega_2) + A''g_1(\omega_2) &= F_2, \end{aligned} \quad (32)$$

where F_1 and F_2 are values of $\text{Re}F(\omega)$ and $\text{Im}F(\omega)$ in the corresponding extrema.

If the function $g(\omega)$ in Eq. 11 is normalized to unity at $\omega = 0$, then setting

$$z = \pi T \omega, \quad \gamma = \pi T \alpha, \quad (33)$$

one has

$$\begin{aligned} g_1(\omega) &= \frac{\cos \gamma z \sinh z + \gamma \sin \gamma \cosh z}{\sinh^2 z + \sin^2 \gamma}, \\ g_2(\omega) &= \frac{\sin \gamma z \cosh z - \gamma \cos \gamma \sinh z}{\sinh^2 z + \sin^2 \gamma}, \\ |g(\omega + i\alpha)|^2 &= \frac{z^2 + \gamma^2}{\sinh^2 z + \sin^2 \gamma}. \end{aligned} \quad (34)$$

It is easy to see that extrema of $g_1(\omega)$ and $|g(\omega + i\alpha)|$ are realized at $\omega = 0$, i.e. they are not affected by finiteness of α , so it is natural to count ω_1 and ω_2 from zero. The function $g_2(\omega)$ is odd and its small addition to $g_1(\omega)$ shifts the extremum to right or left, in dependence on the sign of such addition. In the case of functions $\text{Re}F(\omega)$ and $\text{Im}F(\omega)$, the additions to $g_1(\omega)$, proportional to $g_2(\omega)$, have the opposite signs and provide different signs for ω_1 and ω_2 . For small α one can simplify Eq. 34, retaining the first order in γ , and use the smallness of ω_1 and ω_2 :

$$\tan \varphi = -\frac{\omega_1}{\alpha} = \frac{\alpha}{\omega_2}, \quad \alpha^2 = -\omega_1 \omega_2. \quad (35)$$

In this approximation Eq. 32 gives $A' \approx F_1$, $A'' \approx F_2$, which allows to establish the sign of α and choose the correct quadrant for φ , accepting that the latter belongs to the interval $(-\pi, \pi)$:

$$\alpha = \sqrt{-\omega_1 \omega_2} \text{sign}(\omega_2 F_1 F_2),$$

$$\varphi = -\arctan(\omega_1/\alpha) + \pi \text{sign} F_2 (1 - \text{sign} F_1)/2. \quad (36)$$

It should be stressed that nontrivial information contained in $|\tan \varphi|$ is determined by ω_1 and ω_2 , while F_1 and F_2 are used only for the choice of the correct quadrant. Estimation (36) for φ differs radically from the estimate given in Sec. 7 and coincides with it only in the case, if the shifts of extrema of $\text{Re}F(\omega)$ and $\text{Im}F(\omega)$ are actually related with the exponential growth.

Comparison of two estimations of φ (see Table) demonstrates their approximate agreement for all harmonics and confirms the suggested mechanism for shifts of extrema. Small differences between two estimations may be related with the approximate character of formula (36), and with other factors, such as mutual influence of harmonics, existence of the continuous spectrum, experimental inaccuracies, etc.

Table. Estimations of phases obtained in Sec. 7 (φ_s) and according formula (36) ($\tilde{\varphi}_s$).

s	φ_s	$\tilde{\varphi}_s$	s	φ_s	$\tilde{\varphi}_s$
1	170°	161°	10	37°	37°
2	-88°	-84°	11	155°	145°
3	125°	120°	12	-15°	-20°
4	-172°	-162°	13	111°	121°
5	-78°	-67°	14	-96°	-106°
6	47°	40°	15	-81°	-72°
7	144°	153°	16	87°	84°
8	59°	49°	17	-144°	-140°
9	-124°	-153°			

9. Distribution of the growth exponents and the frequency differences

Let give a summary of theoretical results for evolution of the ρ moments. Accepting that $\langle \rho^n \rangle$ behaves with L as $\exp xL$, we can obtain the algebraic equation of $(2n+1)$ th order for the grow exponent x . For $n = 1$ and $n = 2$ such equations can be given explicitly [8]

$$x(x^2 + 4\mathcal{E}) = 2W^2,$$

$$x(x^2 + 4\mathcal{E})(x^2 + 16\mathcal{E}) = 42W^2x^2 + 96W^2\mathcal{E}, \quad (37)$$

where \mathcal{E} is the energy counted from the lower edge of the initial band, and W is the amplitude of the random potential.

The structure of equations for arbitrary n th moments can be established using argumentation presented in Section 4 in [8]. In the deep of the allowed and forbidden bands, only diagonal elements can be retained in matrices (43) and (47) in [8] and their analogs for higher moments. As a result, we arrive at the equation

$$\prod_{k=0}^{2n} [x - 2(n-k)\delta - B_n^k \epsilon^2] = O(\epsilon^4 \delta^{2n-1}), \quad (38)$$

where $\epsilon^2 = W^2/4\mathcal{E}$, $\delta^2 = -\mathcal{E}$, $B_n^k = n(2n-1) + 3k(k-2n)$. A similar equation near the band edge

$$x^{2n+1} = \sum_{k=0}^{k_{max}} C_k W^{2k} x^{2n+1-3k}, \quad k_{max} = \left\lfloor \frac{2n+1}{3} \right\rfloor \quad (39)$$

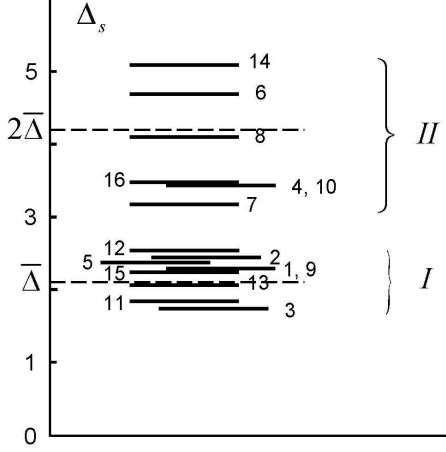


Figure 11: Distribution of differences $\Delta_s = \omega_{s+1} - \omega_s$ between the neighboring frequencies; the s value is indicated near the corresponding lines. Differences Δ_s break up into two groups I and II , localized near $\bar{\Delta}$ and $2\bar{\Delta}$.

follows from observation that all terms of the equation have the same order of magnitude at $x \sim \delta \sim \epsilon^2$ and only combinations $\delta^{2n}\epsilon^{2m}$ with $n \geq m$ are allowed, among which only $\delta^{2n}\epsilon^{2n} \sim W^{2n}$ remain finite at $\delta \rightarrow 0$. Nontrivial roots of Eq. 39 are of the order of $W^{2/3}$ and leads to the incommensurate oscillations in Eq. 2.

In the deep of the allowed band parameters δ and ϵ are complex, and one should make a replacement $\delta \rightarrow i\delta$, $\epsilon \rightarrow -i\epsilon$ in order to reduce them to the real form. Then Eq. 38 gives the complete set of exponents for the extremely metallic regime ($\epsilon^2 \ll \delta$)

$$x_n^k = 2i(n-k)\delta - B_n^k \epsilon^2 + O(\epsilon^4/\delta), \quad k = 0, 1, \dots, 2n. \quad (40)$$

One can see that all frequencies of oscillations in Eq. 2 are integer multiple of the quantity $\bar{\Delta} = 2\delta$, i.e. their incommensurability disappears. In the ideal case all differences of the neighboring frequencies $\Delta_s = \omega_{s+1} - \omega_s$ should be equal to $\bar{\Delta}$. Practically certain harmonics are not manifested due to their weak intensity, so differences Δ_s are "quantized", and may be equal $\bar{\Delta}$, $2\bar{\Delta}$, $3\bar{\Delta}$, etc.

The distribution of differences Δ_s for 17 harmonics, evident from Fig. 3, is represented in Fig. 11. They break up into two groups I and II , localized near $\bar{\Delta}$ and $2\bar{\Delta}$, where $\bar{\Delta}$ is chosen from the best agreement. Absence of exact quantization should not cause any trouble, since it refers only to the extremal metallic regime. In actuality the metallic

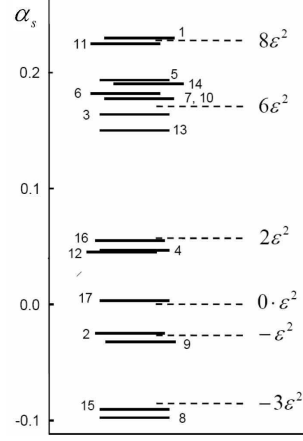


Figure 12: Distribution of the growth exponents α_s and their comparison with succession (41) for the proper choice of ϵ^2 . The s value is indicated near the corresponding lines.

regime is not extremal and the corrections indicated in Eq. 40 become visible.

The growth exponents α_s are determined by the real part of Eq. 40 and are integer multiple of the quantity ϵ^2 . Going over all possible values of n and k , one obtains the infinite succession of exponents, which looks as follows near the origin:

$$\dots, -3\epsilon^2, -\epsilon^2, 0, 2\epsilon^2, 3\epsilon^2, 6\epsilon^2, 8\epsilon^2, \dots \quad (41)$$

The exponents obtained by the treatment of the experimental data according to Eq. 36 are represented in Fig. 12 with the opposite sign⁹ and reproduce this succession rather well for the proper choice of ϵ^2 . The only exclusion is absence of the term $3\epsilon^2$, which is probably related with low intensity of the corresponding spectral lines. Manifestations of only exponents close to zero is naturally explained by the fact that harmonics with large (in modulus) exponents are localized near the ends of the experimental range of magnetic fields and are invisible in its middle.

It should be noted that the maximal exponent for the moment $\langle \rho^n \rangle$ in the forbidden band is realized

⁹ Exponents α_s change their sign in the course of transition from the magnetic field B to the effective system length L (the left and right direction trade their places). When passing from conductance to resistance, there is no change of the α_s signs, since the small fluctuations of two quantities are proportional to each other.

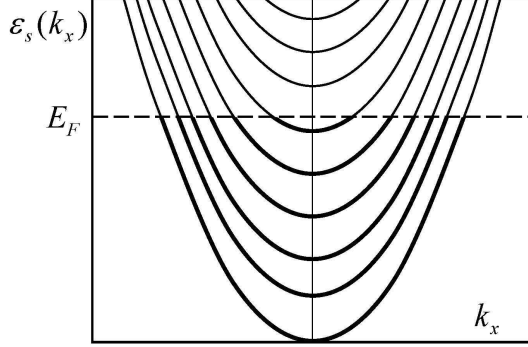


Figure 13: The transverse movement in a thin wire is quantized, so N_0 discrete levels arise, which becomes 1D subbands, if the longitudinal movement is taken into account. The main contribution to the conductance oscillations is given by the upper filled subband.

for $k = 2n$,

$$x_n^{max} = 2n\delta + n(2n - 1)\epsilon^2, \quad (42)$$

and in the allowed band for $k = n$,

$$x_n^{max} = n(n + 1)\epsilon^2. \quad (43)$$

These results are in agreement with the functional form for the log-normal regime

$$x_n^{max} = an + bn^2/2 \quad (44)$$

with parameters a and b , obtained in [8]: $a = 2\delta - \epsilon^2$, $b = 4\epsilon^2$ in the forbidden band, and $a = \epsilon^2$, $b = 2\epsilon^2$ in the allowed band.

10. Microscopical picture

It is easy to see that quantization for the growth exponents α_s (Fig.12) is more exact than for the frequency differences Δ_s (Fig.11). This fact allows a simple explanation.

A thin wire is a quasi-1D system, in which the transverse motion is quantized, so N_0 discrete levels ϵ_s^0 arise. If the longitudinal movement along the x axis is taken into account, the levels transform to the 1D subbands with the spectra

$$\epsilon_s(k_x) = \epsilon_s^0 + k_x^2/2m, \quad (45)$$

whose states are filled below the Fermi level E_F (Fig.13). The magnetic field B affects most strongly

the upper filled subband with the minimal Fermi energy ϵ_F , restricting the movement in it by the length L determined by the condition

$$m\omega_B^2 L^2 \sim \epsilon_F \sim E_0/N_0, \quad (46)$$

so

$$L \sim a \frac{B_0}{B\sqrt{N_0}}, \quad (47)$$

where $E_0 = \hbar^2/ma^2$ and $B_0 = \phi_0/a^2$ are the atomic units of the energy and the magnetic field, while $\phi_0 = \pi\hbar c/e$ is the flux quantum. The system conductance is determined by the sum of the subband conductances, whose oscillations are exponentially decreasing for large L (see below). The main contribution to oscillations is given by the upper filled subband where the length L is minimal, while the neighbouring subbands also have a certain influence. This influence is rather essential for the frequency differences Δ_s and broadens their distribution (Fig.11), since ω_s are determined by the Fermi momentum k_F , whose value is different for different subbands. As for the growth exponents α_s (Fig.12), a situation is strikingly different for them. The Fermi momenta are small for upper subbands, and the approximation of slow particles is applicable for the scattering on impurities¹⁰, so the scattering amplitude is independent of a momentum. The growth exponents are directly related with the scattering amplitude and do not depend on the Fermi momenta of 1D subbands. As a result, the neighbouring subbands do not affect the exact quantization, so Fig.12 corresponds to a strictly 1D system. Deviations from exact quantization are related only with nonextremality of the metallic regime and experimental inaccuracies.

The minimal discrete harmonics in Fig.3 approximately corresponds to 4 oscillations for a change of the magnetic field in the interval $1 \div 10T$. Its frequency is determined by the de Brougli wavelength $\lambda \sim a\sqrt{N_0}$ in the upper subband, while the number of oscillations in the interval of fields from B_{min} till

¹⁰ One should take into account a difference of the actual system from the Anderson model considered in [8]. In the Anderson model, the metallic regime corresponds to a large concentration of weak impurities, which can be treated by perturbation theory. In the actual system, the weak disorder is created by a small concentration of strong impurities, for which the slow particles approximation can be used. This difference does not affect the results for the exponents α_s , since on the scale of a wavelength the configuration of the random potential can be changed in wide limits without influence on the large scale properties of wave functions.

$10B_{min}$ is given by the estimate

$$N_{osc} \sim B_0/N_0B_{min}, \quad (48)$$

following from (47), and setting $B_0 \sim 10^4 T$, $B_{min} = 1T$, $N_{osc} = 4$, one obtains

$$N_0 \sim 2.5 \cdot 10^3. \quad (49)$$

It is half of the number of atoms in the cross section of a wire with 25 nm in diameter [5], and corresponds to a half-filled 3D band. In this case $\lambda \sim 50a$, and the actual length range

$$L = 20 \div 200a \quad (50)$$

is within the wire length 310 nm [5].

Above we accept the condition $\hbar\omega_B \ll \epsilon_F$, which is in fact violated in the middle of the experimental range of magnetic fields. For large fields another estimate $L \sim a(B_0/B)^{1/2}$ is more adequate, which follows from Eq.46 after replacement ϵ_F by $\hbar\omega_B$. As a result, the lower bound in Eq.50 shifts from $20a$ to $30a$, which is not essential for the given estimates.

As clear from Eqs.23,25, the expression for $\langle\rho\rangle$ contains the increasing exponent $e^{2\epsilon^2 l}$ and oscillating terms, decaying as $e^{-\epsilon^2 l}$. The analogous picture is valid for higher moments: the maximal exponent x_n^{max} in the metallic regime is real (see (43)) and is not assisted by oscillations, while the oscillating terms grow more slowly and are relatively small even for positive α_s . As a result, the situation for a typical value of ρ is qualitatively the same as for its moments and, coming to dimensionless conductance $g = 1/\rho$, one finds its oscillations being decreasing. If the typical values $\Delta_1 \sim \Delta_2 \sim 1$ are accepted for the foreign leads, the oscillations of g are of the order of unity in the range $\epsilon^2 l \lesssim 1$, while the dimensional conductance fluctuates on the level of e^2/h (Fig.1). According to this picture, only the order of magnitude of these fluctuations is universal, while their amplitude may be strongly affected by the change of the Fermi level and the properties of the ideal leads.

11. Conclusion

The paper presents the accurate Fourier analysis of aperiodic conductance oscillations discovered in the classical experiments by Webb and Washburn [5]. The obtained results reconcile two alternative scenarios discussed in Sec.1. On one hand, the Fourier spectrum is practically discrete, confirming the conception of the paper [8], according to which

aperiodic oscillations are determined by a superposition of incommensurate harmonics. On the other hand, the spectrum in whole resembles the discrete white noise, whose properties are close to the continuous one. The more detailed analysis reveals existence of the continuous component, whose smallness is theoretically explained in Sec. 5.

The paper discovers a lot of qualitative moments, confirming the presented picture. The frequencies of the discrete harmonics depend very slightly on the treatment procedure, which proves their objective existence. The "natural" origin of the $f(x)$ argument, established after exclusion of the shift oscillations confirms validity of the analogy with 1D systems. The same is confirmed by manifestations of the exponential growth of harmonics. The phase distribution for the coefficients A_s agree with their expected randomness. The distribution of the growth exponents and the differences of neighboring frequencies is in agreement with theoretical results for the metallic regime. Microscopical estimates are in agreement with the geometrical dimensions of the sample.

Universal conductance fluctuations are discussed in a lot of works (see [20–40] and references therein), and it would be interesting to process another experimental data in the spirit of the present paper.

The author is grateful to V.V.Brazhkin, who was an initiator of the paper [11].

Appendix 1. Solution of equation (19)

Let restrict the analysis by the metallic regime, where typical values of ρ are small. Consider the eigenvalue problem for the operator in the right hand side of Eq.19 and, retaining the terms of the lower order in ρ , come to equation

$$-\lambda P = P'_\rho + \rho P''_{\rho\rho}. \quad (A.1)$$

Assuming that ρ changes in the interval from zero till R , let accept the condition of finiteness at $\rho = 0$ and the zero boundary condition at $\rho = R$. Then eigenvalues and eigenfunctions have the form

$$\lambda_s = \mu_s^2/4R, \quad e_s(\rho) = J_0\left(\mu_s\sqrt{\rho/R}\right), \quad (A.2)$$

where μ_s are the roots of the Bessel function $J_0(x)$. Solving Eq.19 with the initial condition (22) by ex-

pansion of $P(\rho)$ over eigenfunctions (A.2), we obtain

$$P(\rho, t) = \int_0^\infty 2\mu d\mu e^{-\mu^2 t} J_0(2\mu\sqrt{\rho_0}) J_0(2\mu\sqrt{\rho}). \quad (\text{A.3})$$

Here we set $t = \alpha(L - L_0)$ and take into account that for large R the spectrum of μ_s becomes quasi-continuous and summation over s may be replaced by integration over μ , using the asymptotics $\mu_s = \pi s + \text{const}$ for large s . Calculating the integral in (A.3), we have

$$P(\rho, t) = \frac{1}{t} \exp\left\{-\frac{\rho + \rho_0}{t}\right\} I_0\left(\frac{2\sqrt{\rho\rho_0}}{t}\right), \quad (\text{A.4})$$

where $I_0(x) = J_0(ix)$. For $\rho \lesssim t$ and $t \gg \rho_0$ distribution (A.4) transforms to (21), while for ρ close to ρ_0 and $t \ll \rho_0$ accepts the Gaussian form

$$P(\rho, t) = \left(\frac{1}{4\pi\rho_0 t}\right)^{1/2} \exp\left\{-\frac{(\rho - \rho_0)^2}{4\rho_0 t}\right\}. \quad (\text{A.5})$$

The closeness of (A.4) to the Gaussian distribution allows to characterize it by two first moments. Multiplying Eq. 19 by ρ^n and integrating over ρ , we have the evolution equation for the moments of the distribution $P(\rho)$; their solution for the initial condition (22) has a form

$$\langle \rho \rangle = -\frac{1}{2} + \frac{1 + 2\rho_0}{2} e^{2t}, \quad (\text{A.6})$$

$$\langle \rho^2 \rangle = \frac{1}{3} - \frac{1 + 2\rho_0}{2} e^{2t} + \left[\rho_0^2 + \frac{1 + 2\rho_0}{2} - \frac{1}{3}\right] e^{6t}.$$

and simplifies for small ρ ,

$$\begin{aligned} \langle \rho \rangle &= \rho_0 + t, \\ \langle \rho^2 \rangle &= \rho_0^2 + 4\rho_0 t + 2t^2, \\ \sigma^2 &= 2\rho_0 t + t^2, \end{aligned} \quad (\text{A.7})$$

in agreement with distribution (A.4). These results are valid for $L > L_0$. Analysis of the interval $0 < L < L_0$ is complicated by necessity to satisfy two conditions (20) and (22), which is possible only under certain restrictions on the realization of the random potential. Such restrictions should be imposed on the interval $(0, L_0)$ in whole, and are not essential for small L , and L close to L_0 . In the former case we have $\langle \rho \rangle = \sigma$ in correspondence with distribution (21). In the latter case the situation is

determined by the fact that spreading of the distribution occurs symmetrically¹¹ for deviations of L to left or to right from L_0 . As for the quantity $\langle \rho \rangle$, conditions (20) and (22) are satisfied automatically, if ρ_0 coincides with the mean value of distribution (21) for $L = L_0$. The situation does not change qualitatively, if a typical value from distribution (21) is chosen for ρ_0 . As a result, we come to the picture presented in Fig. 8.

Appendix 2. Evolution of $\langle \rho \rangle$ for the general initial condition

Calculation of $\langle \rho \rangle$ is reduced technically to the study of evolution of the second moments for the transfer matrix with complex elements T_{ij} [8]

$$\begin{aligned} z_1^{(l)} &= \left\langle |T_{11}^{(l)}|^2 \right\rangle, & z_2^{(l)} &= \left\langle T_{11}^{(l)} T_{12}^{(l)*} \right\rangle, \\ z_3^{(l)} &= \left\langle T_{11}^{(l)*} T_{12}^{(l)} \right\rangle, & z_4^{(l)} &= \left\langle |T_{12}^{(l)}|^2 \right\rangle, \end{aligned} \quad (\text{A.8})$$

They satisfy the system of difference equations, whose general solution has a form [8]

$$\begin{pmatrix} z_1^{(l)} \\ z_2^{(l)} \\ z_3^{(l)} \\ z_4^{(l)} \end{pmatrix} = C_0 \begin{pmatrix} -1 \\ 0 \\ 0 \\ 1 \end{pmatrix} + \sum_{i=1}^3 C_i \begin{pmatrix} 1 \\ e_2(x_i) \\ e_3(x_i) \\ 1 \end{pmatrix} \exp(x_i l), \quad (\text{A.9})$$

where x_1, x_2, x_3 are the roots of the first equation (37), and

$$\begin{aligned} e_2(x) &= \frac{\mathcal{A}x + \mathcal{B}}{p(x)}, & e_3(x) &= \frac{\mathcal{A}^*x + \mathcal{B}^*}{p(x)}, \\ \mathcal{A} &= 2\epsilon^2 - 2i\Delta, & \mathcal{B} &= 4\alpha\Delta + 4i\epsilon^2(\alpha - \Delta), \\ p(x) &= x^2 + 2\epsilon^2 x + 4\alpha^2. \end{aligned} \quad (\text{A.10})$$

Here $\alpha = -\Delta_2\delta$, $\Delta = \Delta_1\delta$, while δ and ϵ^2 are defined after (23), and

$$\Delta_1 = \frac{1}{2} \left(\frac{k}{\bar{k}} - \frac{\bar{k}}{k} \right), \quad \Delta_2 = \frac{1}{2} \left(\frac{k}{\bar{k}} + \frac{\bar{k}}{k} \right). \quad (\text{A.11})$$

where \bar{k} and k are Fermi momenta in the system under consideration and in the ideal leads connected to

¹¹ Equation (19) has the same form, if we set $L = L_0 + l$ or $L = L_0 - l$ and consider evolution over l . It is clear from the derivation scheme of such equations (see Appendix A in [41]).

it. In contrast to [8], we accept the initial condition not in the form of the unit matrix, but as the general transfer matrix

$$T = \begin{pmatrix} \sqrt{\rho+1} e^{i\varphi} & \sqrt{\rho} e^{i\theta} \\ \sqrt{\rho} e^{-i\theta} & \sqrt{\rho+1} e^{-i\varphi} \end{pmatrix}, \quad (A.12)$$

with $\rho = \rho_0$ and $\psi = \theta - \varphi$. The quantity $z_4^{(l)}$ immediately determines $\langle \rho \rangle$, and the general result for the latter has a form

$$\langle \rho \rangle = C_0 + C_1 e^{x_1 l} + C_2 e^{x_2 l} + C_3 e^{x_3 l}, \quad (A.13)$$

where

$$C_0 = -\frac{1}{2}, \quad C_i = (-1)^{i+1} \left[(1+2\rho_0) \frac{Q_i}{2Q} + K_1 \frac{R_i}{Q} + K_2 \frac{S_i}{Q} \right], \quad i = 1, 2, 3 \quad (A.14)$$

and

$$\begin{aligned} Q_1 &= (x_2 - x_3) p(x_1), \quad Q_2 = (x_1 - x_3) p(x_2), \\ Q_3 &= (x_1 - x_2) p(x_3), \\ Q &= Q_1 - Q_2 + Q_3 = x_1^2 (x_2 - x_3) - x_2^2 (x_1 - x_3) + x_3^2 (x_1 - x_2) \\ R_1 &= [x_2 p(x_3) - x_3 p(x_2)] p(x_1), \\ R_2 &= [x_1 p(x_3) - x_3 p(x_1)] p(x_2), \\ R_3 &= [x_1 p(x_2) - x_2 p(x_1)] p(x_3), \\ S_1 &= [p(x_3) - p(x_2)] p(x_1), \\ S_2 &= [p(x_3) - p(x_1)] p(x_2), \\ S_3 &= [p(x_2) - p(x_1)] p(x_3), \\ K_1 &= \frac{\epsilon^2 \sin \psi - \Delta \cos \psi}{4[\alpha \Delta^2 + \epsilon^4(\alpha - \Delta)]} \sqrt{\rho_0(1 + \rho_0)}, \quad (A.15) \\ K_2 &= \frac{\epsilon^2(\alpha - \Delta) \cos \psi + \alpha \Delta \sin \psi}{2[\alpha \Delta^2 + \epsilon^4(\alpha - \Delta)]} \sqrt{\rho_0(1 + \rho_0)}. \end{aligned}$$

Using asymptotic forms for x_1, x_2, x_3 in the metallic regime [8], we come to results (23) and (25). The first result is valid for the "natural" ideal leads¹², which differ from the system under consideration only by absence of the random potential in them; in this case $k = \bar{k}$, $\Delta_1 = 0$ and oscillations occur in the first order in the small parameter ϵ^2/δ . Result (25) is valid for foreign leads, when $\Delta_1 \neq 0$ and oscillations occur in the zero order in ϵ^2/δ . The use

¹² In this case, the roots x_1, x_2, x_3 should be expanded in ϵ^2/δ to the higher order than in the paper [8].

of the asymptotic results for x_1, x_2, x_3 in the "critical" region [8] leads to result (24), applicable near the edge of the initial band; it is given for the "natural" leads, since the situation for the foreign leads is sufficiently illustrated by the formulas presented in [8].

Appendix 3. On the choice of the natural x origin

According to the Onsager relations, conductance is an even function of the magnetic field B and accepting $x = B$ one has an even function $f(x)$ in Eq.3. Let accept the smoothing function in the x -symmetrized form $G(x-a) + G(x+a)$ with even $G(x)$. Then the Fourier transform is real and apart the sign coincides with its modulus, so it does not contain the shift oscillations. Now let remove the function $G(x+a)$. The arising Fourier transform $F(\omega)$ of the function $f(x)G(x-a)$ appears to be complex, with its real part being half of the previous¹³, and free of the shift oscillations. The latter will be absent also in $\text{Im } F(\omega)$, since they affect equally the real and imaginary parts. After the shift $x \rightarrow x+a$ the Fourier transform looks as follows

$$F(\omega) = e^{i\omega a} \int f(x+a)G(x)e^{i\omega x} dx$$

and the arising integral for $a = \mu_0$ corresponds to the integral considered in Sec.2, while the factor $e^{i\omega a}$ produces shift oscillations. However, the obtained sign of a is opposite to that found empirically.

The origin of the contradiction lies in the fact that the Onsager symmetry distinguishes not only value $B = 0$ but also $B = \infty$, and just the latter corresponds to the empirical situation. Indeed, accepting $x = 1/B$, we can repeat the previous argumentation, but now the decrements of B and x have opposite signs, and for the qualitative correspondence with Sec.2 the sign of ω should be changed. As a result, the factor $\exp\{i\omega a\}$ has a correct sign of a .

References

- [1] B. L. Altshuler, JETP Lett. **41**, 648 (1985) [Pis'ma Zh. Eksp. Teor. Fiz. **41**, 530 (1985)];

¹³ One can verify easily that the Fourier transforms of functions $f(x)G(x+a)$ and $f(x)G(x-a)$ have equal real and opposite imaginary parts.

- [2] B. L. Altshuler, D. E. Khmelnitskii, JETP Lett. **42**, 359 (1985) [Pis'ma Zh. Eksp. Teor. Fiz. **42**, 291 (1985)].
- [3] P. A. Lee, A. D. Stone, Phys. Rev. Lett. **55**, 1622 (1985).
- [4] P. A. Lee, A. D. Stone, H. Fukuyama, Phys. Rev. B **35**, 1039 (1987).
- [5] S. Washburn, R. A. Webb, Adv. Phys. **35**, 375 (1986).
- [6] B. L. Altshuler, P. A. Lee, R. A. Webb (Eds), Mesoscopic Phenomena in Solids, North-Holland, Amsterdam, 1991.
- [7] C. W. J. Beenakker, Rev. Mod. Phys. **69**, 731 (1997).
- [8] I. M. Suslov, J. Exp. Theor. Phys. **129**, 877 (2019); [Zh. Eksp. Teor. Fiz. **156**, 950 (2019)].
- [9] L. D. Landau, E. M. Lifshitz, Quantum Mechanics, Pergamon, 1977.
- [10] D. Mailly, M. Sanquer, J. Phys. (France) I **2**, 357 (1992).
- [11] V. V. Brazhkin, I. M. Suslov, J. Phys.: Condensed Matter (in print); Arxiv: 1911.10441.
- [12] W. H. Press, B. P. Flannery, S. A. Teukolsky, W. T. Vetterling, Numerical Recipes in Fortran, Cambridge University Press, 1992.
- [13] A. B. Migdal, Qualitative Methods in Quantum Theory, Nauka, Moscow, 1975.
- [14] V. I. Melnikov, Sov. Phys. Sol. St. **23**, 444 (1981) [Fizika Tverdogo Tela **23**, 782 (1981)].
- [15] A. A. Abrikosov, Sol. St. Comm. **37**, 997 (1981).
- [16] N. Kumar, Phys. Rev. B **31**, 5513 (1985).
- [17] B. Shapiro, Phys. Rev. B **34**, 4394 (1986).
- [18] P. Mello, Phys. Rev. B **35**, 1082 (1987).
- [19] B. Shapiro, Phil. Mag. **56**, 1031 (1987).
- [20] K. M. D. Hals, A. K. Nguyen, X. Waintal, A. Brataas, Phys. Rev. Lett. **105**, 207204 (2010).
- [21] A. S. Lien, L. Y. Wang, C. S. Chu, J. J. Lin, Phys. Rev. B **84**, 155432 (2011).
- [22] J. G. G. S. Ramos, D. Bazeia, M. S. Hussein, C. H. Lewenkopf, Phys. Rev. Lett. **107**, 176807 (2011).
- [23] Z. Li, T. Chen, H. Pan, et al, Sci. Rep. **2**, 595 (2012).
- [24] E. Rossi, J. H. Bardarson, M. S. Fuhrer, S. D. Sarma, Phys. Rev. Lett. **109**, 096801 (2012).
- [25] P. Y. Yang, L. Y. Wang, Y. W. Hsu, J. J. Lin, Phys. Rev. B **85**, 085423 (2012).
- [26] S. Minke, J. Bundesmann, D. Weiss, J. Eroms, Phys. Rev. B **86**, 155403 (2012).
- [27] S. Gustavsson, J. Bylander, W. D. Oliver, Phys. Rev. Lett. **110**, 016603 (2013).
- [28] A. L. R. Barbosa, M. S. Hussein, J. G. G. S. Ramos, Phys. Rev. E **88**, 010901(R) (2013).
- [29] Ph. Jacquod and I. Adagideli, Phys. Rev. B **88**, 041305(R) (2013).
- [30] J. Bundesmann, M. H. Liu, I. Adagideli, K. Richter, Phys. Rev. B **88**, 195406 (2013).
- [31] C. L. Richardson, S. D. Edkins, G. R. Berdiyorov, et al, Phys. Rev. B **91**, 245418 (2015).
- [32] T. C. Vasconcelos, J. G. G. S. Ramos, A. L. R. Barbosa, Phys. Rev. B **93**, 115120 (2016).
- [33] C. C. Kalmbach, F. J. Ahlers, J. Schurr, et al, Phys. Rev. B **94**, 205430 (2016).
- [34] J. G. G. S. Ramos, A. L. R. Barbosa, B. V. Carlson, et al, Phys. Rev. E **93**, 012210 (2016).
- [35] Y. Hu, H. Liu, H. Jiang, X. C. Xie, Phys. Rev. B **96**, 134201 (2017).
- [36] H. C. Hsu, I. Klefogiannis, G. Y. Guo, V. A. Gopar, J. Phys. Soc. Jpn **87**, 034701 (2018).
- [37] M. A. Aamir, P. Karnatak, A. Jayaraman, et al, Phys. Rev. Lett. **121**(13), 136806 (2018).
- [38] S. Islam, S. Bhattacharyya, H. Nhalil, et al, Phys. Rev. B **97**, 241412R (2018).
- [39] T. Vercosa, Y. J. Doh, J. G. G. S. Ramos, A. L. R. Barbosa, Phys. Rev. B **98**, 155407 (2018).
- [40] F. Hajiloo, F. Hassler, J. Splettstoesser, Phys. Rev. B **99**, 235422 (2019).
- [41] I. M. Suslov, J. Exp. Theor. Phys. **124**, 763 (2017) [Zh. Eksp. Teor. Fiz. **151**, 897 (2017)].